Check for updates

ORIGINAL PAPER

CRYSTAL Research & Technology

www.crt-journal.org

Crystal Growth of Materials with the $ThCr_2Si_2$ Structure Type

*Kristin Kliemt, Marius Peters, Fabian Feldmann, Alexej Kraiker, Doan-My Tran, Susanna Rongstock, Johannes Hellwig, Sebastian Witt, Michael Bolte, and Cornelius Krellner**

The single crystal growth of 19 different intermetallic compounds within the LnT_2X_2 family (with Ln = lanthanides, T = Co, Ru, Rh, Ir, and X = Si, P) is presented, by employing a high-temperature metal-flux technique. The habitus of the obtained crystals is platelet-like with the crystallographic *c* direction perpendicular to the surface and with individual masses between 1 and 100 mg. The magnetic properties of these crystals are characterized by magnetization, heat-capacity, and resistivity measurements. These crystals form the materials basis for a thorough study of exciting surface properties by angle-resolved photoemission spectroscopy.

1. Introduction

The interaction of valence electrons with a lattice of localized 4*f* states is responsible for intriguing electronic states and phase transitions under variation of temperature and pressure. Within these materials, the ternary intermetallic LnT_2X_2 family (with Ln = lanthanides, T = transition metal and X = element from the carbon or nitrogen group) in the $ThCr_2Si_2$ structure type[1,2] stands out, because many examples of emergent correlated phenomena were discovered in compounds with this structure type. Prominent examples are $CeCu_2Si_2$, the first unconventional superconductor,[3] URu_2Si_2, the famous hidden-order superconductor,[4] $YbRh_2Si_2$ a prototypical material to explore quantum criticality,[5] AFe_2As_2 materials, the parent compounds of the "122"-family of Fe-based superconductors,[6,7] as well as the first valence fluctuating system $EuCu_2Si_2$.[8]

Dr. K. Kliemt, M. Peters, F. Feldmann, A. Kraiker, D.-M. Tran, S. Rongstock, J. Hellwig, S. Witt, Prof. C. Krellner
Kristall- und Materiallabor
Physikalisches Institut
Goethe-Universität Frankfurt
60438 Frankfurt, Main, Germany
E-mail: krellner@physik.uni-frankfurt.de

Dr. M. Bolte
Institut für Anorganische und Analytische Chemie
Goethe-Universität Frankfurt
60438 Frankfurt, Main, Germany

The ORCID identification number(s) for the author(s) of this article can be found under https://doi.org/10.1002/crat.201900116

© 2019 The Authors. Published by WILEY-VCH Verlag GmbH & Co. KGaA, Weinheim. This is an open access article under the terms of the Creative Commons Attribution-NonCommercial-NoDerivs License, which permits use and distribution in any medium, provided the original work is properly cited, the use is non-commercial and no modifications or adaptations are made.

DOI: 10.1002/crat.201900116

The characteristics of this structure are layers of edge-connected TX_4-tetrahedra, which alternate along the *c* direction with planar square lattices of Ln-atoms (see **Figure 1**). For $LnIr_2Si_2$ compounds, often polymorphism with two different structure types, $ThCr_2Si_2$ (*I*4/*mmm*) and $CaBe_2Ge_2$ (*P*4/*nmm*) is observed.[9–12] In the latter, an Ir- and Si-plane are interchanged with each other, leading to a lower symmetry, with a missing mirror plane at the body-centered Ln-atom (see e.g., Figure 1 in ref. [13]). This structure is therefore named primitive (or P-type) in contrast to the body-centered (I-type) version. In the studied cases, the body-centered $ThCr_2Si_2$-type structure is the thermodynamically stable variant at low temperature, whereas the primitive $CaBe_2Ge_2$-type structure is formed only at high temperature. A further peculiarity of the $ThCr_2Si_2$ structure is the transition into the so-called collapsed tetragonal phase with strongly reduced X-X distances compared to the normal tetragonal phase of these materials. This transition was observed for X = P, As and deeply investigated in Fe-based superconductors, as, for example, $CaFe_2As_2$, where this transition is induced by external pressure.[14]

In some of the Fe- or Co-based 122 superconductors with the $ThCr_2Si_2$ structure type, pronounced deviations from the ideal stoichiometry are observed. Examples are $LaCo_xAs_2$ with x ranging from $1.6 \leq x \leq 2.1$[15] as well as $K_xFe_{2-y}Se_2$ with $0.2 \leq x \leq 1$ and $y \leq 0.4$.[16,17] In those cases, a careful structural and chemical determination of the precise stoichiometry is necessary. A further indication of strong off-stoichiometry is a very low residual resistivity ratio (RRR) which is below 1.5 in $LaCo_xAs_2$ and $K_xFe_{2-y}Se_2$.[16,17] In the LnT_2Si_2 compounds, such strong deviations from the ideal stoichiometry have not been observed; however, for the materials close to a quantum critical point (QCP) as $CeCu_2Si_2$ and $YbRh_2Si_2$ even very small deviations in the stoichiometry can lead to changes in the physical properties. This is due to the nearly degenerate ground states close to the QCP. There, a very careful examination of the stoichiometry with a feedback to the crystal growth parameters needs to be undertaken to allow the fabrication of crystals with well-defined physical properties. For $CeCu_2Si_2$ this took quite some time and it was found that the Cu/Si ratio can slightly vary from $CeCu_{2.03}Si_{1.97}$ to $CeCu_{2.05}Si_{1.95}$. This is accompanied by a change from an antiferromagnetic ground state to a superconducting one.[18] In $YbRh_2Si_2$ a finite homogeneity range for the Rh/Si ratio was found as well through accurate X-ray diffraction and wavelength dispersive X-ray spectroscopy measurements, although it turned out to be very small, $z \leq 0.01$ in $YbRh_{2+z}Si_{2-z}$.[19] Remarkably, the

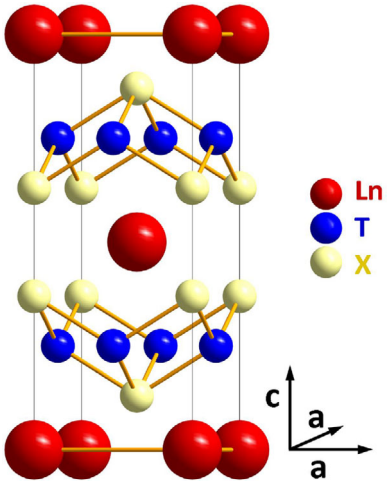

Figure 1. Tetragonal $ThCr_2Si_2$ structure type of the LnT_2X_2 materials.

accompanied defects could be visualized in real space by scanning tunneling microscopy and have strong impact on the RRR and the temperature dependence of the resistivity close to the QCP.[13]

The magnetic properties of the presented ternary intermetallic LnT_2X_2 materials are mainly due to the magnetism of Ln, with exception of the materials with T = Co. Some of them were already studied in great detail in recent years – others not. We started this work with the crystal growth of the heavy-fermion compounds $YbRh_2Si_2$ and $YbIr_2Si_2$.[13] These crystals were investigated in detail by thermodynamic measurements at mK temperatures and turned out to be very convenient for angle-resolved photoemission spectroscopy (ARPES).[20,21] The platelet-like crystals can be easily cleaved to obtain a well-defined surface, crucial for ARPES. After the discovery of strong ferromagnetism at the surface of the antiferromagnetic $EuRh_2Si_2$ by ARPES,[22] this opened the way for a systematic investigation of the surface states in $LnRh_2Si_2$ and $LnIr_2Si_2$ using this technique.[23–27] These surface states were found to be strongly modified by the internal magnetic fields from the ordered rare earth ions underneath and for a thorough understanding of these effects it is essential to characterize the magnetic ground state in great detail.

In this overview, we will present the results of the crystal growth of 19 different compounds together with their structural and magnetic properties, which partly were not reported yet in literature.

2. Crystal Growth

Growing crystals of compounds with high-melting transition metals (like Ru, Rh, or Ir) on the one hand and elements with high vapor pressure (like P or Yb) on the other hand is often a difficult challenge. One attractive method to overcome this is to use a low-melting metallic flux (such as In or Sn). By using a flux it is possible to solve the high-melting elements as well as the elements with low boiling points and obtain a melt with a moderate vapor pressure which is suitable for the growth. A good overview about the use of metallic fluxes is given in refs. [28–30]. In the past, the flux method has been successfully applied for intermetallic compounds using indium, tin or lithium as flux.[30–34] In some cases, the use of a solvent leads to the formation of unwanted phases; in this regard the use of a self-flux can be more successful. Even when using a flux, the growth temperature often exceeds 1200 °C. Due to the highly volatile and reactive constituents, the growth then usually is performed in a closed niobium or tantalum crucible. For the silicides presented in this work an indium flux was used, whereas for the phosphides the successful growths were performed with tin. Furthermore, we used an inner crucible made from graphite, enclosed under argon in the Ta- or Nb-crucible.

Often the Bridgman technique is used to grow single crystals of congruent melting materials. In the conventional Bridgman technique, the crystallization of a sample is controlled by moving an ampoule which contains the molten educts through a temperature gradient. The ampoule is moved from the hot to the colder zone of a tubular furnace. During cooling, a growth front between melt and solid forms, where the crystallization takes place. One disadvantage of this method is the direct contact of the material with the crucible, which can cause strain and defects in the grown single crystal. Furthermore, the crucible material can be attacked by the melt. For the crystal growth of LnT_2X_2 compounds, presented in this work, we used a modified Bridgman method in a vertical resistive furnace (GERO HTRV70250/18) in which a maximum temperature of 1700 °C can be used. This method was optimized in great detail for the crystal growth of the heavy-fermion compounds $YbRh_2Si_2$ and $YbIr_2Si_2$[13] and later successfully applied to other compounds as presented in **Table 1**.

In our experiments, the crucible is placed on a sample holder which remains on a fixed position. To achieve crystallization, the furnace is moved upwards. This setup is advantageous, since the furnace is decoupled from the sample holder and the sample does not experience vibrations due to the motion of the furnace. At the beginning of the growth, the furnace heated up to the maximum furnace temperature of $T_{max} = 1550$ °C with a rate of 300 K h^{-1} for the silicides. After a homogenization period of 1 h, the furnace moved upward applying a fast-move period ($v = 100$ mm h^{-1}) followed by a slow-move period ($v = 1$ mm h^{-1}). The fast-move period after homogenization is necessary to quickly lower the temperature at the bottom of the crucible. Long exposure at high temperatures might lead to enhanced pollution of the melt with material from the crucible. During the slow-move period, the crystal growth takes place. Afterward, the furnace cooled down with 200 K h^{-1} to room temperature. A typical temperature-time profile for $LnRh_2Si_2$ is shown in Figure 1 of ref. [35]. For the iridium compounds, the cooling was performed with a lower cooling rate ($\Delta T = 50$ K h^{-1}) than for the rhodium compounds ($\Delta T = 200$ K h^{-1}). The idea was to include an annealing period, to obtain crystals with the low-temperature $ThCr_2Si_2$-type crystal structure $I4/mmm$. For the P-based compounds, which were grown in Sn-flux, the maximum furnace temperature was lower (1300 to 1400 °C) and the initial heat-up rate was slower (100 K h^{-1}) with an additional hold time of 10 h at 450 °C, to ensure a complete reaction of P with Sn. A flow of argon through the growth tube was present (≈ 150 mL min^{-1}) for all the experiments, which prevented oxidation of the metallic crucible and provided an additional cooling at the bottom of the crucible. The indium and tin flux was removed after the growth by etching with hydrochloric acid.

© 2019 The Authors. Published by WILEY-VCH Verlag GmbH & Co. KGaA, Weinheim

Table 1. Structural properties of the grown crystals within the LnT_2X_2 family. $\bar{m}$ denotes the average mass of the 10 largest crystals obtained in each growth. The quality of the crystals is reflected in the resistivity ratio (RR) measured with current perpendicular to the *c* direction, $RR = \rho_{300K}/\rho_{1.8K}$. For materials with low lying phase transitions, as, for example, $YbRh_2Si_2$, the residual resistivity ratio, $RRR = \rho_{300K}/\rho_{0K}$ can be much higher. The RR value for current parallel to the *c* direction is lower, but could not be systematically determined due to the reduced thickness of the crystals. "long edge" refers to the longest naturally grown edge which can vary between [100] and [110] for the different materials. If the probability for the long edge to be [110] or [100] is nearly equal, this is denoted by "mixed." Directions marked with an asterisk are found with 80% probability. The lattice parameters are taken from literature. For $GdIr_2Si_2$ and $LuIr_2Si_2$ they were obtained within this work.

LnT_2X_2	$\bar{m}$ [mg]	RR $j \perp c$	long edge	a [Å]	c [Å]	Ref.
$PrRh_2Si_2$	10	18	[110]	4.079	10.138	[36]
$NdRh_2Si_2$	5	25	[110]	4.069	10.11	[37]
$SmRh_2Si_2$	1	25	[100]	4.055	10.04	[38]
$GdRh_2Si_2$	25	23	[110]*	4.042	9.986	[39]
$TbRh_2Si_2$	7	13	mixed	4.037	9.95	[37]
$DyRh_2Si_2$	60	10	[110]	4.022	9.90	[37]
$HoRh_2Si_2$	11	15	[110]	4.015	9.89	[37]
$TmRh_2Si_2$	35	15	mixed	4.01	9.85	[40]
$YbRh_2Si_2$	50	30	[110]*	4.007	9.862	[19]
$LuRh_2Si_2$	1	6	[110]*	4.000	9.87	[37]
$GdIr_2Si_2$	5	30	[100]	4.060	9.930	
$TbIr_2Si_2$	4	47	[100]	4.143	10.155	[41]
$DyIr_2Si_2$	3	38	[100]	4.029	9.856	[42]
$HoIr_2Si_2$	30	29	[100]	4.048	9.884	[43]
$YbIr_2Si_2$	40	95	[100]	4.035	9.828	[13]
$LuIr_2Si_2$	1	1.2	[100]	4.031	9.807	
$LaCo_2P_2$	6	11	[100]	3.815	11.04	[44]
$CeCo_2P_2$	14	2.4	[100]	3.895	9.604	[44]
$CeRu_2P_2$	4	56	[110]*	4.042	10.134	[45]

In an ideal growth experiment, solidification should start at the coldest point, the tip at the bottom of the crucible. Afterward, the crystal should grow from the tip. Ideally, this should prevent further nucleation in the crucible. But in our experiments the formation of many small crystals was observed. An explanation for this could be the constitutional undercooling of the melt. An improvement of the mixing of the melt, for example, by rotating the crucible could prevent the strong undercooling. In these experiments it is not possible to use a seed in the present setup since the cooling with a gas flow at the lower part of the crucible is not strong enough to avoid that the seed is dissolved by the melt. However, in our case, it is advantageous that in one batch a few tens of crystals grow, because many crystals are needed due to repeated cleaving procedures in ARPES measurements.

The average mass and the resistivity ratio given in Table 1 reveal strong differences for the various materials. The different values are likely due to the different solubilities of the starting materials in the flux at a given temperature. An individualized optimization of the initial stoichiometry and the temperature profile would be required for each material, to obtain higher values. For $YbRh_2Si_2$ such an extensive optimization revealed that three times excess of Yb was necessary to grow crystals which are thicker than 0.1 mm along the crystallographic *c* direction, leading to an initial stoichiometry of the melt of 3 : 2.2 : 1.8 : 24 (Yb : Rh : Si : In).[13] For the other LnT_2Si_2 compounds presented in Table 1, we used an initial stoichiometry of 1 : 2 : 2 : 24 (Ln : T : Si : In). For $GdIr_2Si_2$, the optimization of the growth conditions to obtain single crystals in the low temperature phase ($I4/mmm$) and large enough to be suited for ARPES studies turned out to be more elaborate. Finally, we found that the $I4/mmm$ phase forms if the initial stoichiometry of the melt was chosen to be 1 : 2 : 2 : 49 (Gd : Ir : Si : In). The high-temperature phase ($P4/nmm$) was formed in experiments with an initial stoichiometry of 1.1 : 0.9 : 0.9 : 24 (Gd : Ir : Si : In). For the Co-based compounds, we optimized the initial stoichiometry with tin flux and obtained good results for 1.6 : 2 : 2 : 30 (Ln : Co : P : Sn), whereas for $CeRu_2P_2$ we used the stoichiometry 1 : 1 : 1 : 57 (Ce : Ru : P : Sn).

3. Structural and Chemical Characterization

The single crystals of LnT_2X_2 grown with the high-temperature metal-flux technique all had a platelet-like habitus (see **Figure 2**b–f). Their individual masses range from 1 to 100 mg (see Table 1). To give a quantitative measure, we have determined an average mass, $\bar{m}$, weighing the 10 largest crystals obtained in each growth. The crystal structure was confirmed to be of $ThCr_2Si_2$ type by powder X-ray diffraction. For that purpose we have taken selected crystals and powdered them. The diffraction patterns were recorded on a diffractometer with Bragg–Brentano

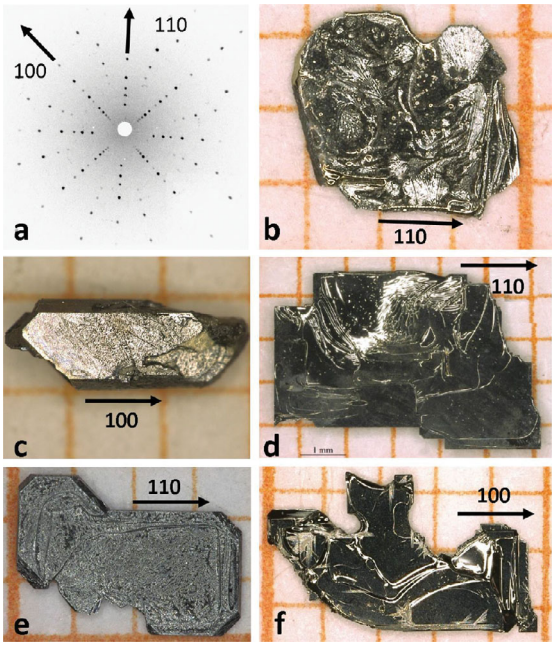

Figure 2. a) Laue pattern of $TbRh_2Si_2$ and single crystals of b) $TbRh_2Si_2$, c) $TbIr_2Si_2$, d) $HoRh_2Si_2$, e) $CeRu_2P_2$, and f) $CeCo_2P_2$. The largest surface of the crystals is always perpendicular to the crystallographic *c* direction, but the direction of the longest edges can differ for the different materials. The underlying grid is in all cases millimeter paper.

© 2019 The Authors. Published by WILEY-VCH Verlag GmbH & Co. KGaA, Weinheim

geometry and copper K_α radiation. The Laue method was used to determine the orientation of the crystals relative to an X-ray beam from a tungsten anode. Additionally, the shapes of the obtained reflections provide information on the crystallinity of the single crystal. For $TbRh_2Si_2$ an example is shown in Figure 2a, with sharp and well-defined spots. The fourfold symmetry of the *c* axis which is perpendicular to the surface of the crystals is clearly visible. Simulation of the Laue patterns of LnT_2Si_2 revealed, that the spots along the [100] direction appear closer to the (001) point compared to the [110] direction (Figure 2a). The pictures of the crystals together with their orientations in Figure 2 b–f show, that the longest naturally grown edge can vary between [100] and [110] for the different materials. On the other hand, the shortest edge, that is, the direction perpendicular to the surface of the platelets, is always along [001]. In Table 1, the preferences of the long edge for the different materials are given. It turned out that for the compounds with T = Ir and Co, the longest edge is always along [100], whereas for T = Rh this can vary. There, in some cases it can even vary from crystal to crystal in one batch, sometimes with a higher probability to find the [110] direction ($GdRh_2Si_2$, $YbRh_2Si_2$, $LuRh_2Si_2$, $CeRu_2P_2$) and sometimes with similar probabilities ($TbRh_2Si_2$ and $TmRh_2Si_2$). The reason for that observation is the similar binding energies for the two in-plane directions, but a much smaller one for the *c* direction.

The chemical compositions of the single crystals were analyzed by energy-dispersive X-ray spectroscopy (EDX) and revealed for the presented silicides values of (20±1)at% Ln, (40±1)at% T, and (40±2)at% Si. From these measurements, we can exclude strong non-stoichiometry in the presented materials, as it was observed in $LaCo_2As_2$[15] and KFe_2Se_2.[16,17] However, we cannot exclude small homogeneity ranges as it was observed for $CeCu_2Si_2$[18] and $YbRh_2Si_2$.[19] For the Co-based compounds $LaCo_2P_2$ and $CeCo_2P_2$, we observed slightly off-stoichiometric values. We measured several crystals from different batches and obtained (19±1)at% Ln, (37±1)at% Co, and (44±2)at% P. For $CeRu_2P_2$, we observed similar values as in the silicides and obtained (19±1)at% Ce, (40±1)at% Ru, and (41±2)at% P. The absence of pronounced non-stoichiometry in the silicides and in $CeRu_2P_2$ is further confirmed by rather high RR values (typically larger than 10, see Table 1). One exception is $LuIr_2Si_2$, where we might have pronounced structural disorder, probably Ir-Si side exchanges which is not detectable in chemical analysis. As discussed in the introduction, the P-type structure can be formed in $LnIr_2Si_2$ systems. The difference to the I-type structure is one Ir-Si layer with interchanged Ir-Si position (see e.g., Figure 1 in ref. [13]). The observed off-stoichiometry in $LnCo_2P_2$ is confirmed by low RR values for these two compounds. For $LaCo_2P_2$ crystals with higher RR has been grown by Teruya et al.,[46]; therefore, this is not an intrinsic property of this material and might be improved by optimization of the initial stoichiometry and the temperature profile during the crystal growth.

For $GdIr_2Si_2$ we have performed a single crystal structure determination of the I-type crystal. The data were collected at 173 K on a STOE IPDS II two-circle diffractometer with a Genix Microfocus tube with mirror optics using MoK_α radiation ($\lambda = 0.71073$ Å) and were scaled using the frame scaling procedure in the X-AREA program system.[47] The structure was solved by direct methods using the program SHELXS[48] and refined against F^2 with full-matrix least-squares techniques using the program SHELXL.[48] The atomic coordinates determined by single crystal analysis are summarized in **Table 2**. The lattice parameters are shown in Table 1. In the refinement, we tested interchanged Ir-Si positions as defects but could not detect them. This is in agreement with a rather high RR = 30 for this compound.

Table 2. Atomic coordinates and equivalent isotropic displacement parameters for $GdIr_2Si_2$ (*I*4/*mmm*) determined by single crystal analysis at $T = 173$ K. U(eq) is defined as one third of the trace of the orthogonalized U^{ij} tensor.

Atom	Wyckoff position	*x*	*y*	*z*	*U*(eq) [Å^2]
Gd	2a	0	0	0	0.032(1)
Ir	4d	0	0.5	0.25	0.031(1)
Si	4e	0	0	0.3761(9)	0.033(2)

4. Physical Characterization

Now, we focus on the magnetic properties of the different LnT_2X_2 materials. With the exception of $LnCo_2P_2$, the magnetism in these compounds arises solely from the trivalent rare earth ions and can be characterized as local-moment magnetism due to the spatially localized character of the 4*f*-wave functions. These magnetic moments polarize the spins of the conduction electrons which mediate the magnetic exchange interaction (RKKY), leading to long-range magnetic order with ordering temperatures of several tens of K. In case of Yb and Ce-based systems, the Kondo effect can lead to a screening of the magnetic moments, resulting in a suppression of magnetic order. In **Table 3**, an overview of the magnetic structures of these compounds is presented, which in most cases were determined by neutron diffraction, reported in literature in recent years. As discussed in the introduction, these materials can be cleaved easily and were therefore extensively studied by ARPES. It was found that the electronic surface states are strongly modified by the internal magnetic fields from the ordered rare earth ions. For a thorough understanding of these magnetic effects on the surface states it is essential to characterize the magnetic ground state in detail. We therefore measured magnetization, heat capacity, and resistivity for most of the materials in Table 3 and will show some of these measurements in the following.

The physical properties presented in this work were all measured in a commercial Physical Property Measurement System (PPMS) from Quantum Design, equipped with a 9 T magnet enabling fast temperature control from 1.8 to 400 K. A vibrational sample magnetometer (VSM option) was used to measure the magnetization as function of temperature or field. This option was additionally equipped with a local heater stick to measure up to 800 K. The resistivity was obtained with the AC-transport option in a four-point geometry. The contacts were manually prepared on the surface of the crystals with silver epoxy and 25 µm thick Pt wire. Heat-capacity measurements were performed with a thermal-relaxation method.

In **Figure 3**, we present heat-capacity and resistivity measurements of $TbRh_2Si_2$ and $TbIr_2Si_2$. In the heat capacity, pronounced anomalies are visible at the antiferromagnetic transition

© 2019 The Authors. Published by WILEY-VCH Verlag GmbH & Co. KGaA, Weinheim

Table 3. Magnetic properties of the LnT_2X_2 compounds. Given is the magnetic ordering temperature T_N and the corresponding ordering vector $\vec{k}$. If a second magnetic ordering appears at lower temperatures, this is given as T_{N_2}. Furthermore, the direction of the magnetic moment within the ordered phase is given. The magnetic ordering temperatures were obtained from thermodynamic measurements within this work. *nk* stands for *not known*.

LnT_2X_2	T_N [K]	$\vec{k}_{T_N}$	T_{N_2} [K]	$\vec{k}_{T_{N_2}}$	Mom. direc.	Ref.
$PrRh_2Si_2$	68	(001)	—	—	$\parallel c$	[36]
$NdRh_2Si_2$	58	(001)	—	—	$\parallel c$	[49]
$SmRh_2Si_2$	64	*nk*	—	—	$\perp c$	[38]
$GdRh_2Si_2$	107	(001)	—	—	$\perp c$	[39]
$TbRh_2Si_2$	94	(001)	—	—	$\parallel c$	[41]
$DyRh_2Si_2$	52	(001)	18	(001)	$\parallel c$[a)]	[50]
$HoRh_2Si_2$	29	(001)	11	(001)	$\parallel c$[b)]	[51]
$TmRh_2Si_2$	6.4	*nk*	4	*nk*	$\parallel c$[c)]	[40]
$YbRh_2Si_2$	0.07	*nk*	—	—	*nk*	[52]
$LuRh_2Si_2$	—	—	—	—	—	[53]
$GdIr_2Si_2$	86	*nk*	—	—	$\perp c$	this work
$TbIr_2Si_2$	82	(001)	—	—	$\parallel c$	[41]
$DyIr_2Si_2$	42	(001)	10[d)]	(001)	$\parallel c$	[42]
$HoIr_2Si_2$	22	(001)	—	—	$\parallel c$	[43]
$YbIr_2Si_2$	—	—	—	—	—	[54]
$LuIr_2Si_2$	—	—	—	—	—	[54]
$LaCo_2P_2$	135[e)]	FM	—	—	$\perp c$	[55]
$CeCo_2P_2$	440	*nk*	—	—	*nk*	[44]
$CeRu_2P_2$	—	—	—	—	—	[56]

[a)] Below T_{N_2} a canting of the moment sets in, which reaches $\approx 19°$ at 4.2 K; [b)] $HoRh_2Si_2$ presents three magnetic transitions. An additional one at 27 K. Between 29 and 27 K the ordering vector is unknown. Below T_{N_2} a canting of the moment sets in, which reaches $\approx 32°$ at 1.5 K; [c)] Only one magnetic transition was reported in ref. [40], with the direction of the magnetic moment canted $\approx 68°$ away from *c* at 4.2 K; [d)] Only one magnetic transition was reported in ref. [42], with the direction of the magnetic moment along *c* at 1.5 K; [e)] This compound orders ferromagnetically (FM) and we found a much higher T_C in agreement with ref. [57], but in contrast to $T_C = 103$ K reported in ref. [55].

($T_N^{Rh} = 94$ K, $T_N^{Ir} = 82$ K), which were first reported on polycrystalline samples in neutron diffraction by Slaski et al.[41]. Below T_N no further anomaly is visible down to 1.8 K for both compounds. For comparison, the heat-capacity data of the non-magnetic $LuRh_2Si_2$ and $LuIr_2Si_2$ are shown as solid lines. From the comparison of these curves it is obvious that the difference of $TbRh_2Si_2$ and $TbIr_2Si_2$ above T_N comes from differences in the phonon contribution to the heat capacity, as this difference is also observable in the non-magnetic references. The electrical resistivity for both compounds shows an anomaly at the same magnetic ordering temperature as the heat-capacity. Below T_N, the drop is stronger for $TbIr_2Si_2$, indicating a smaller residual resistivity at lower temperatures. This is reflected in a higher resistivity ratio, RR = 47, for $TbIr_2Si_2$ compared to RR = 13 for $TbRh_2Si_2$. No sizable anisotropy was detected for $TbIr_2Si_2$, when measuring the resistivity with current along and perpendicular to the crystallographic *c* direction (open and closed symbols, respectively in Figure 3b).

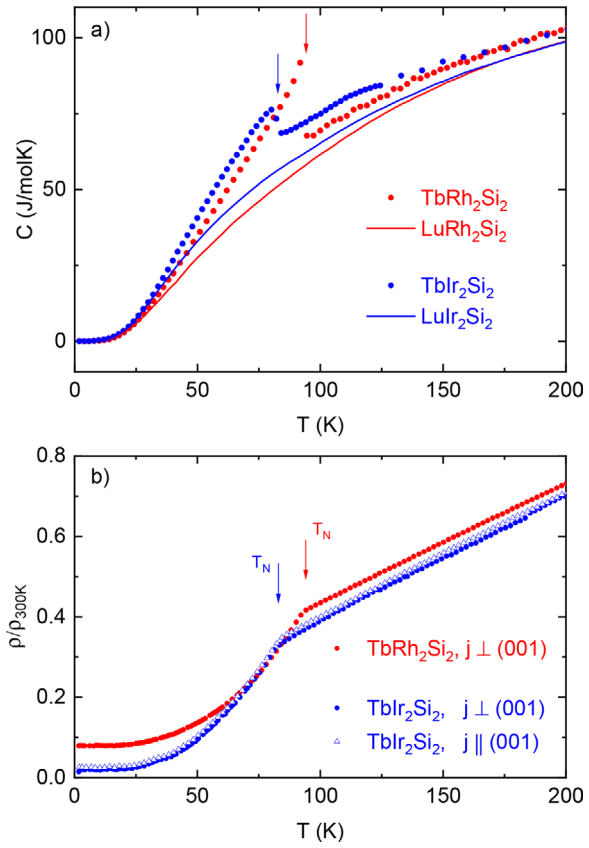

Figure 3. a) Heat capacity and b) resistivity normalized to 300 K of $TbRh_2Si_2$ and $TbIr_2Si_2$ single crystals. For comparison, the data of the heat capacity for $LuRh_2Si_2$[53] and $LuIr_2Si_2$ are shown as solid lines in (a).

The magnetic properties of $TmRh_2Si_2$ were poorly documented in literature and so far, to the best of our knowledge, only one neutron study on polycrystalline samples at 4.2 K has been reported.[40] In **Figure 4**a, we present heat-capacity measurements of $TmRh_2Si_2$ and found two sharp anomalies at $T_N = 6.4$ K and $T_{N_2} = 4.0$ K. The shape of the anomalies might indicate a first-order transition of the latter, although we could not detect latent heat directly in the temperature–time relaxation curves. The temperature dependence of the resistivity confirms the conclusion drawn from heat-capacity measurements. Above 10 K, the system behaves as an ordinary metal and at T_N a pronounced drop indicates the onset of magnetic order, followed by a smaller drop at T_{N_2}. Extrapolating the resistivity down to zero temperature, we obtain a RRR = 17, which indicates that disorder does not play an important role in this compound.

As discussed in the introduction, some of the $LnIr_2Si_2$ compounds present two structural variants. In **Figure 5**, we present heat-capacity and resistivity measurements on single crystals of the two different polymorphs of $GdIr_2Si_2$. In literature, magnetic properties have only been reported for the $ThCr_2Si_2$ structure type ($I4/mmm$), with an antiferromagnetic transition at $T_N = 82.4$ K.[63] In agreement to that, we found antiferromagnetic order at $T_N = 86$ K for the $I4/mmm$ compound, whereas the compound with the $CaBe_2Ge_2$ structure type ($P4/nmm$) orders antiferromagnetically at $T_N = 12.5$ K. The $P4/nmm$

© 2019 The Authors. Published by WILEY-VCH Verlag GmbH & Co. KGaA, Weinheim

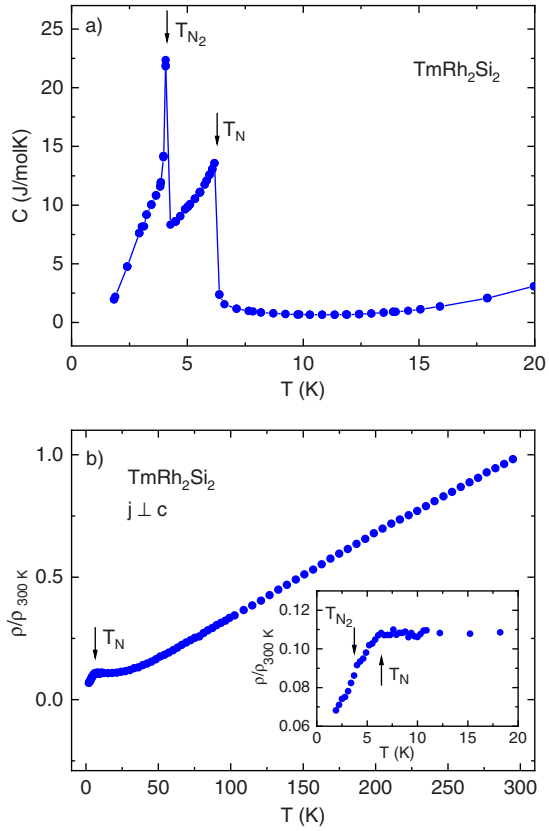

Figure 4. a) Heat capacity and b) resistivity normalized to 300 K of $TmRh_2Si_2$ single crystals. In the heat-capacity measurements two well-defined anomalies indicate the onset of long-range magnetic ordering. At T_N a pronounced drop is seen in the resistivity followed by a smaller kink at T_{N_2}.

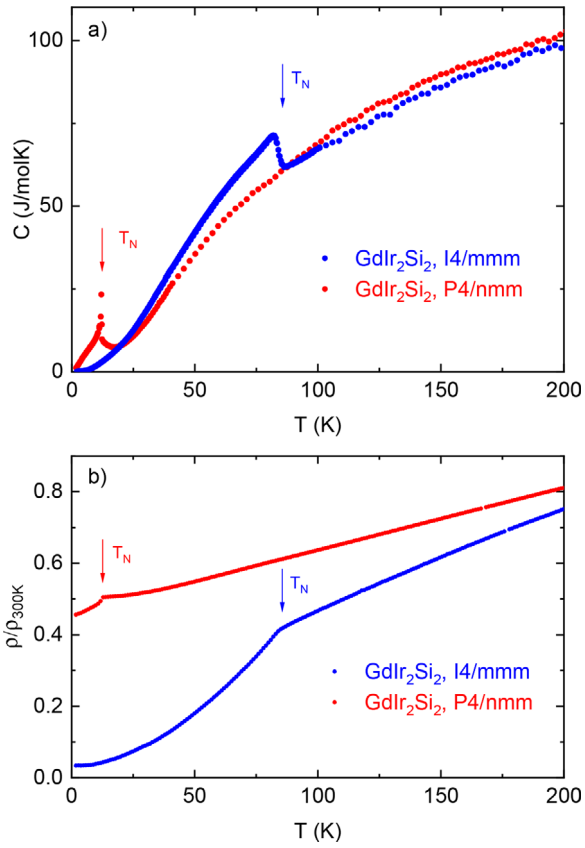

Figure 5. a) Heat capacity and b) resistivity normalized to 300 K for the two structural polymorphs of $GdIr_2Si_2$. The one with the $ThCr_2Si_2$ structure type (*I*4/*mmm*, blue symbols) presents antiferromagnetic order at 86 K. The one with the $CaBe_2Ge_2$ structure type (*P*4/*nmm*, red symbols) orders at 12.5 K. In the resistivity measurements current was applied perpendicular to the *c* direction.

compound shows a rather high degree of disorder, resulting in a low RRR = 2.2, whereas the *I*4/*mmm* compound has a RRR = 30. This is typical for the two structural polymorphs, because the *P*4/*nmm* phase is only metastable at room temperature and cooling down after the crystal growth, probably results in some Ir-Si side exchanges. Similar different RRR values with different magnetic ground states were observed for the two polymorphs of $YbIr_2Si_2$.[64]

The magnetic ordering of the $LnRh_2Si_2$ and $LnIr_2Si_2$ series can be understood in terms of RKKY theory. There, the size of the interaction energy depends on the distances between the magnetic atoms and the Fermi wave vector, which would need *ab initio* band-structure calculations to determine it. In cases where a sizable *f*–*d* hybridization leads to strongly correlated systems, this is not an easy task. An alternative way is to relate the ordering temperatures to the de Gennes factor $dG = [(g_J - 1)^2 J(J + 1)]$, a parameter derived for the size of exchange interaction, where g_J is the Landè *g* factor and *J* is the total angular momentum of the Ln^{3+} ions (with a ground state *J* according to the three Hund's rules). In **Figure 6**, we have plotted the magnetic ordering temperatures of the $LnRh_2Si_2$ and $LnIr_2Si_2$ series as function of atomic number together with *dG*. It is apparent that for the heavy rare-earth atoms ($Z \geq 64$) the scaling is valid, whereas it completely fails for the light rare-earth atoms ($Z \leq 63$). This was also

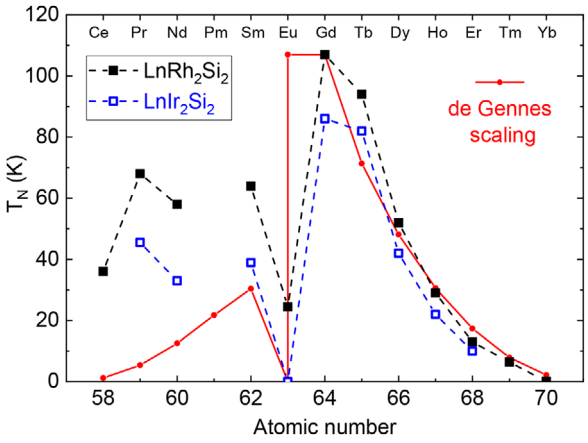

Figure 6. Magnetic ordering temperatures of $LnRh_2Si_2$ (closed symbols) and $LnIr_2Si_2$ (open symbols) as function of the atomic number. For comparison, the de Gennes factor multiplied by the highest ordering temperature (T_N = 107 K for $GdRh_2Si_2$) is shown as solid line. For Eu two values of the de Gennes temperature are shown, zero for Eu^{3+} and 107 K for Eu^{2+}, because Eu is divalent with long-range magnetic order in $EuRh_2Si_2$ but trivalent (non-magnetic) in $EuIr_2Si_2$. The ordering temperatures are taken from Table 3 and from references[42,58–62].

© 2019 The Authors. Published by WILEY-VCH Verlag GmbH & Co. KGaA, Weinheim

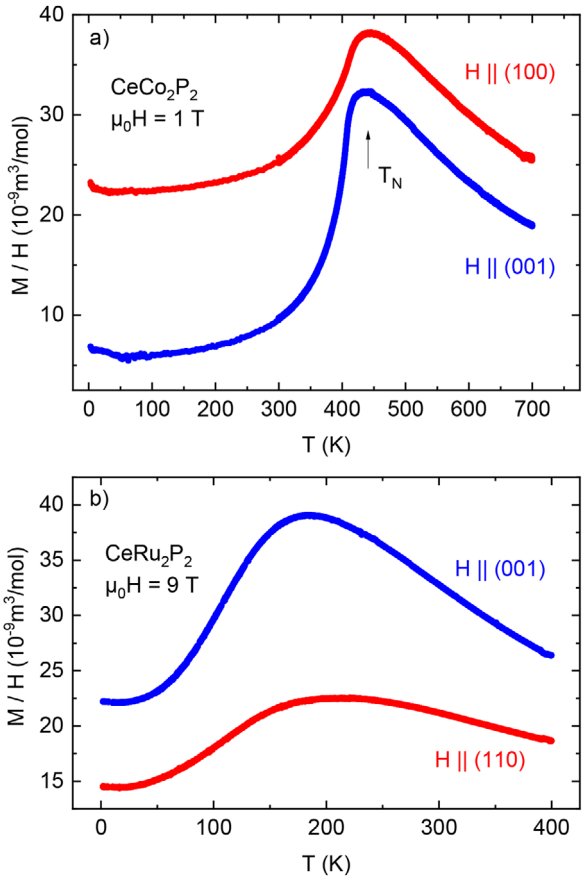

Figure 7. Susceptibility (dc) as function of temperature for a) $CeCo_2P_2$ and b) $CeRu_2P_2$ single crystals.

observed in other rare-earth series and is likely due to stronger hybridization of *f* and conduction (*spd*) electrons as well as stronger influence of the crystalline electric field for the lighter rare earths, with more extended 4*f* wave functions.

In the final part of this section, we now turn to the P-based materials. $CeCo_2P_2$ was first characterized by Reehuis and Jeitschko[44] and found to be antiferromagnetic at 440 K due to ordering of the *d*-electrons of cobalt. This was later on confirmed by neutron powder diffraction experiments, which revealed that the Co-atoms are ordered ferromagnetically within the basal plane and antiferromagnetically along the *c* axis.[65] In contrast, the ordering of $LaCo_2P_2$ is ferromagnetic below 135 K, with the moments pointing along the [100] direction.[55] One open question concerns the large ordering temperature in $CeCo_2P_2$, which is four times higher compared to $LaCo_2P_2$. One possibility would be a contribution to the magnetic exchange from the 4*f*-electrons. However, the development of the unit cell volume through the lanthanide series $LnCo_2P_2$ suggests a tetravalent or intermediate valent Ce ground state at 300 K. However, at higher temperatures, a strong increase of the unit-cell volume was observed, indicating a tendency toward more trivalent Ce.[65] In **Figure 7**a, we present the dc susceptibility M/H of a $CeCo_2P_2$ single crystal in a wide temperature range from 2 to 700 K for two field directions. For both field directions, the susceptibility increases with decreasing temperature above T_N, followed by a pronounced decrease below T_N. The susceptibility perpendicular to the *c* direction is larger in the complete temperature range compared to the susceptibility measured with field along *c*. At 700 K, the magnetic anisotropy is about 1.35, whereas in the ordered phase it increases to about 4. The magnetic anisotropy in the ordered phase is in agreement with the moments pointing along the *c* direction as concluded from neutron diffraction; however, the sizable anisotropy above T_N is unexpected if the magnetic behavior would be only due to itinerant *d* magnetism of Co. For example, in $LaCo_2P_2$ there is little anisotropy in the spin fluctuations above T_C[57] and also in $SrCo_2P_2$ no sizable magnetic anisotropy was detected at 300 K.[66] Therefore, it is reasonable to assume that Ce is not completely tetravalent above 300 K and that the observed anisotropy comes from some remaining 4*f* magnetism.

This conclusion is confirmed when looking at the magnetic anisotropy in $CeRu_2P_2$, shown in Figure 7b. $CeRu_2P_2$ is an intermediate valent Ce system, with a characteristic energy of the 4*f* electronic system of the order of 200 K, as evidenced by a broad maximum in the electrical resistivity.[56] This energy scale is also visible in the magnetic susceptibility again as a broad maximum at around 200 K (Figure 7b). The intermediate valence of Ce in this compound was recently directly confirmed by X-ray absorption spectroscopy and resonant inelastic X-ray scattering.[67] The magnetic anisotropy of $CeRu_2P_2$ is reversed to $CeCo_2P_2$ with the *c* direction as the easy axis. However, the overall size of the magnetic anisotropy is around 1.5 and therefore similar as observed for $CeCo_2P_2$ above T_N.

5. Conclusion

We have shown that the high-temperature metal-flux technique is an appropriate method for the crystal-growth of LnT_2X_2 materials. We performed an optimization of the initial stoichiometries and temperature profiles for three different material classes, $LnRh_2Si_2$, $LnIr_2Si_2$, and LnT_2P_2 and obtained platelet-like single crystals with masses between 1 and 100 mg. The magnetic properties of these materials vary and we have determined the ordering temperatures by means of magnetization, heat-capacity, and resistivity measurements. We found two magnetic transitions in $TmRh_2Si_2$ at $T_N = 6.4$ K and $T_{N_2} = 4.0$ K. For $GdIr_2Si_2$, single crystals of two different structure types ($ThCr_2Si_2$ and $CaBe_2Ge_2$) were grown, which have different magnetic ordering temperatures at $T_N = 86$ K and $T_N = 12.5$ K, respectively. Finally, we observed magnetic anisotropy in the itinerant 3*d*-magnet $CeCo_2P_2$ above $T_N = 440$ K and attributed this to some remaining 4*f* magnetism, similar to what was observed in the intermediate valent $CeRu_2P_2$. In the future, the presented crystal-growth method will be applied to grow additional LnT_2P_2 compounds, to allow a detailed study of their structural and magnetic properties.

Acknowledgements

The authors thank K. D. Luther and F. Ritter for excellent technical support. We further acknowledge discussions with C. Geibel, D. V. Vyalikh, K. Kummer, and W. Assmus, as well as funding by the DFG through grant KR3831/4-1, KR3831/5-1, and Fermi-NESt.

© 2019 The Authors. Published by WILEY-VCH Verlag GmbH & Co. KGaA, Weinheim

Conflict of Interest

The authors declare no conflict of interest.

Keywords

correlated electrons, flux growth, magnetism, $TmRh_2Si_2$, $GdIr_2Si_2$

Received: June 14, 2019
Revised: August 26, 2019
Published online: October 15, 2019

[1] Z. Ban, M. Sikirica, *Acta Crystallogr.* **1965**, *18*, 594.
[2] R. Hoffmann, C. Zheng, *J. Phys. Chem.* **1985**, *89*, 4175.
[3] F. Steglich, J. Aarts, C. D. Bredl, W. Lieke, D. Meschede, W. Franz, H. Schäfer, *Phys. Rev. Lett.* **1979**, *43*, 1892.
[4] T. T. M. Palstra, A. A. Menovsky, J. v. d. Berg, A. J. Dirkmaat, P. H. Kes, G. J. Nieuwenhuys, J. A. Mydosh, *Phys. Rev. Lett.* **1985**, *55*, 2727.
[5] E. Schuberth, M. Tippmann, L. Steinke, S. Lausberg, A. Steppke, M. Brando, C. Krellner, C. Geibel, R. Yu, Q. Si, F. Steglich, *Science* **2016**, *351*, 485.
[6] M. Rotter, M. Tegel, D. Johrendt, *Phys. Rev. Lett.* **2008**, *101*, 107006.
[7] C. Krellner, N. Caroca-Canales, A. Jesche, H. Rosner, A. Ormeci, C. Geibel, *Phys. Rev. B* **2008**, *78*, 100504.
[8] E. R. Bauminger, D. Froindlich, I. Nowik, S. Ofer, I. Felner, I. Mayer, *Phys. Rev. Lett.* **1973**, *30*, 1053.
[9] H. F. Braun, N. Engel, E. Parthé, *Phys. Rev. B* **1983**, *28*, 1389.
[10] W. X. Zhong, B. Lloret, W. L. Ng, B. Chevalier, J. Etourneau, P. Hagenmuller, *Rev. Chim. Miner.* **1985**, *22*, 711.
[11] D. Niepmann, R. Pöttgen, *Intermetallics* **2001**, *9*, 313.
[12] T. Shigeoka, Y. Kurata, T. Nakata, T. Fujiwara, K. Matsubayashi, Y. Uwatoko, *Physics Procedia* **2015**, *75*, 837.
[13] C. Krellner, S. Taube, T. Westerkamp, Z. Hossain, C. Geibel, *Philos. Mag.* **2012**, *92*, 2508.
[14] A. Kreyssig, M. A. Green, Y. Lee, G. D. Samolyuk, P. Zajdel, J. W. Lynn, S. L. Bud'ko, M. S. Torikachvili, N. Ni, S. Nandi, J. B. Leâo, S. J. Poulton, D. N. Argyriou, B. N. Harmon, R. J. McQueeney, P. C. Canfield, A. I. Goldman, *Phys. Rev. B* **2008**, *78*, 184517.
[15] S. Shen, G. Wang, S. Jin, Q. Huang, T. Ying, D. Li, X. Lai, T. Zhou, H. Zhang, Z. Lin, X. Wu, X. Chen, *Chem. Mater.* **2014**, *26*, 6221.
[16] J. Guo, S. Jin, G. Wang, S. Wang, K. Zhu, T. Zhou, M. He, X. Chen, *Phys. Rev. B* **2010**, *82*, 180520.
[17] Y. Liu, G. Wang, T. Ying, X. Lai, S. Jin, N. Liu, J. Hu, X. Chen, *Adv. Sci.* **2016**, *3*, 1600098.
[18] S. Seiro, M. Deppe, H. Jeevan, U. Burkhardt, C. Geibel, *Phys. Status Solidi B* **2010**, *247*, 614.
[19] S. Wirth, S. Ernst, R. Cardoso-Gil, H. Borrmann, S. Seiro, C. Krellner, C. Geibel, S. Kirchner, U. Burkhardt, Y. Grin, F. Steglich, *J. Phys.: Condens. Matter* **2012**, *24*, 294203.
[20] S. Danzenbächer, Y. Kucherenko, D. V. Vyalikh, M. Holder, C. Laubschat, A. N. Yaresko, C. Krellner, Z. Hossain, C. Geibel, X. J. Zhou, W. L. Yang, N. Mannella, Z. Hussain, Z. X. Shen, M. Shi, L. Patthey, S. L. Molodtsov, *Phys. Rev. B* **2007**, *75*, 045109.
[21] D. V. Vyalikh, S. Danzenbächer, A. N. Yaresko, M. Holder, Y. Kucherenko, C. Laubschat, C. Krellner, Z. Hossain, C. Geibel, M. Shi, L. Patthey, S. L. Molodtsov, *Phys. Rev. Lett.* **2008**, *100*, 056402.
[22] A. Chikina, M. Höppner, S. Seiro, K. Kummer, S. Danzenbächer, S. Patil, A. Generalov, M. Güttler, Y. Kucherenko, E. V. Chulkov, Y. M. Koroteev, M. Köpernik, C. Geibel, M. Shi, M. Radovic, C. Laubschat, D. V. Vyalikh, *Nat. Commun.* **2014**, *5*, 3171.
[23] M. Güttler, A. Generalov, M. M. Otrokov, K. Kummer, K. Kliemt, A. Fedorov, A. Chikina, S. Danzenbächer, S. Schulz, E. V. Chulkov, Y. M. Koroteev, N. Caroca-Canales, M. Shi, M. Radovic, C. Geibel, C. Laubschat, P. Dudin, T. K. Kim, M. Hoesch, C. Krellner, D. V. Vyalikh, *Sci. Rep.* **2016**, *6*, 24254.
[24] A. Generalov, M. M. Otrokov, A. Chikina, K. Kliemt, K. Kummer, M. Höppner, M. Güttler, S. Seiro, A. Fedorov, S. Schulz, S. Danzenbächer, E. V. Chulkov, C. Geibel, C. Laubschat, P. Dudin, M. Hoesch, T. Kim, M. Radovic, M. Shi, N. C. Plumb, C. Krellner, D. V. Vyalikh, *Nano Lett.* **2017**, *17*, 811.
[25] A. Chikina, A. Generalov, K. Kummer, M. Güttler, V. N. Antonov, Y. Kucherenko, K. Kliemt, C. Krellner, S. Danzenbächer, T. Kim, P. Dudin, C. Geibel, C. Laubschat, D. V. Vyalikh, *Phys. Rev. B* **2017**, *95*, 155127.
[26] A. Generalov, J. Falke, I. A. Nechaev, M. M. Otrokov, M. Güttler, A. Chikina, K. Kliemt, S. Seiro, K. Kummer, S. Danzenbächer, D. Usachov, T. K. Kim, P. Dudin, E. V. Chulkov, C. Laubschat, C. Geibel, C. Krellner, D. V. Vyalikh, *Phys. Rev. B* **2018**, *98*, 115157.
[27] S. Schulz, I. A. Nechaev, M. Güttler, G. Poelchen, A. Generalov, S. Danzenbächer, A. Chikina, S. Seiro, K. Kliemt, A. Y. Vyazovskaya, T. K. Kim, P. Dudin, E. V. Chulkov, C. Laubschat, E. E. Krasovskii, C. Geibel, C. Krellner, K. Kummer, D. V. Vyalikh, *npj Quantum Mater.* **2019**, *4*, 26.
[28] P. C. Canfield, Z. Fisk, *Philos. Mag. B* **1992**, *65*, 1117.
[29] P. C. Canfield, I. R. Fisher, *J. Cryst. Growth* **2001**, *225*, 155.
[30] M. G. Kanatzidis, R. Pöttgen, W. Jeitschko, *Angew. Chem. Int. Ed.* **2005**, *44*, 6996.
[31] Y. Ônuki, R. Settai, K. Sugiyama, Y. Inada, T. Takeuchi, Y. Haga, E. Yamamoto, H. Harima, H. Yamagami, *J. Phys.: Condens. Matter* **2007**, *19*, 125203.
[32] S. Seiro, C. Geibel, *J. Phys.: Condens. Matter* **2014**, *26*, 046002.
[33] C. Krellner, C. Geibel, *J. Cryst. Growth* **2008**, *310*, 1875.
[34] A. Jesche, P. C. Canfield, *Philos. Mag.* **2014**, *94*, 2372.
[35] K. Kliemt, C. Krellner, *J. Cryst. Growth* **2015**, *419*, 37.
[36] V. K. Anand, Z. Hossain, G. Behr, G. Chen, M. Nicklas, C. Geibel, *J. Phys.: Condens. Matter* **2007**, *19*, 506205.
[37] I. Felner, I. Nowik, *Solid State Commun.* **1983**, *831*, 47.
[38] K. Kliemt, J. Banda, C. Geibel, M. Brando, C. Krellner, **2019**, arXiv:1905.00716.
[39] K. Kliemt, M. Hofmann-Kliemt, K. Kummer, F. Yakhou-Harris, C. Krellner, C. Geibel, *Phys. Rev. B* **2017**, *95*, 134403.
[40] J. Yakinthos, *J. Phys. France* **1986**, *47*, 673.
[41] M. Slaski, J. Leciejewicz, A. Szytuła, *J. Magn. Magn. Mater.* **1983**, *39*, 268.
[42] J. P. Sanchez, A. Blaise, E. Ressouche, B. Malaman, G. Venturini, K. Tomala, R. Kmieć, *J. Magn. Magn. Mater.* **1993**, *128*, 295.
[43] K. Kliemt, M. Bolte, C. Krellner, *J. Phys.: Condens. Matter* **2018**, *30*, 385801.
[44] M. Reehuis, W. Jeitschko, *J. Phys. Chem. Solids* **1990**, *51*, 961.
[45] W. Jeitschko, R. Glaumn, L. Boonk, *J. Sol. State Chem.* **1987**, *69*, 93.
[46] A. Teruya, A. Nakamura, T. Takeuchi, F. Honda, D. Aoki, H. Harima, K. Uchima, M. Hedo, T. Nakama, Y. Onuki, *Phys. Proc.* **2015**, *75*, 876.
[47] Stoe, C. GmbH, Diffractometer control program system (X-AREA, 2002).
[48] G. M. Sheldrick, *Acta Crystallogr. Sect. A* **2008**, *64*, 112.
[49] J. Leciejewicz, H. Ptasiewicz-Bak, A. Szytula, M. Slaski, *Physica B + C* **1985**, *130*, 382.
[50] M. Melamud, H. Pinto, I. Felner, H. Shaked, *J. Appl. Phys.* **1984**, *55*, 2034.
[51] T. Jaworska-Gołab, Ł. Gondek, A. Szytuła, A. Zygmunt, B. Penc, J. Leciejewicz, S. Baran, N. Stüsser, *J. Phys.: Condens. Matter* **2002**, *14*, 5315.
[52] O. Trovarelli, C. Geibel, S. Mederle, C. Langhammer, F. Grosche, P. Gegenwart, M. Lang, G. Sparn, F. Steglich, *Phys. Rev. Lett.* **2000**, *85*, 626.

© 2019 The Authors. Published by WILEY-VCH Verlag GmbH & Co. KGaA, Weinheim

[53] J. Ferstl, New Yb-based systems: From an intermediate-valent to a magnetically ordered state (PhD thesis, TU Dresden, Cuvillier Göttingen, 2007).
[54] Z. Hossain, C. Geibel, F. Weickert, T. Radu, Y. Tokiwa, H. Jeevan, P. Gegenwart, F. Steglich, *Phys. Rev. B* **2005**, *72*, 094411.
[55] M. Reehuis, C. Ritter, R. Ballou, W. Jeitschko, *J. Magn. Magn. Mater.* **1994**, *138*, 85.
[56] T. Fujiwara, K. Kanto, K. Matsubayashi, Y. Uwatoko, T. Shigeoka, *J. Phys.: Conf. Ser.* **2011**, *273*, 012112.
[57] M. Imai, C. Michioka, H. Ueda, K. Yoshimura, *Phys. Rev. B* **2015**, *91*, 184414.
[58] T. Graf, M. F. Hundley, R. Modler, R. Movshovich, J. D. Thompson, D. Mandrus, R. A. Fisher, N. E. Phillips, *Phys. Rev. B* **1998**, *57*, 7442.
[59] S. Seiro, C. Geibel, *J. Phys.: Condens. Mat.* **2011**, *23*, 375601.
[60] A. Szytula, M. Slaski, H. Ptasiewicz-Bak, J. Leciejewicz, A. Zygmunt, *Solid State Communications* **1984**, *52*, 395.
[61] R. Welter, K. Halich, B. Malaman, *J. Alloy. Compd.* **2003**, *353*, 48.
[62] M. Valiska, J. Pospisil, J. Prokleska, M. Divis, A. Rudajevova, I. Turek, V. Sechovsky, *J. Alloy. Compd.* **2013**, *574*, 459.
[63] L. Tung, J. Franse, K. Buschow, P. Brommer, N. Thuy, *J. Alloy. Compd.* **1997**, *260*, 35.
[64] Z. Hossain, C. Geibel, T. Radu, Y. Tokiwa, F. Weickert, C. Krellner, H. Jeevan, P. Gegenwart, F. Steglich, *Physica B* **2006**, *378–380*, 74.
[65] M. Reehuis, W. Jeitschko, G. Kotzyba, B. Zimmer, X. Hu, *J. Alloy. Compd.* **1998**, *266*, 54.
[66] A. Teruya, A. Nakamura, T. Takeuchi, H. Harima, K. Uchima, M. Hedo, T. Nakama, Y. Onuki, *J. Phys. Soc. Jpn.* **2014**, *83*, 113702.
[67] A. Amorese, G. Dellea, M. Fanciulli, S. Seiro, C. Geibel, C. Krellner, I. P. Makarova, L. Braicovich, G. Ghiringhelli, D. V. Vyalikh, N. B. Brookes, K. Kummer, *Phys. Rev. B* **2016**, *93*, 165134.

© 2019 The Authors. Published by WILEY-VCH Verlag GmbH & Co. KGaA, Weinheim